

THE $^{12}\text{C}(\alpha, n)^{15}\text{O}$ AND $^{16}\text{O}(\alpha, n)^{19}\text{Ne}$ REACTIONS AT $E_\alpha = 41$ MeV

D.J. OVERWAY and W.C. PARKINSON

Department of Physics, The University of Michigan, Ann Arbor, Michigan 48109, USA

Received 26 November 1980

Abstract: Spectra and neutron angular distributions have been obtained for the (α, n) reaction on ^{12}C and ^{16}O to (a) determine whether with this reaction more detailed spectroscopic information can be extracted than from heavy-ion induced ^3He transfer reactions, and (b) to compare the results obtained for (α, n) with those from the (α, p) reaction on the same target nuclei. The results indicate that the same states are populated in (α, n) as in the heavy-ion induced reactions; and that the (α, n) results agree with expectations based on the (α, p) reaction at $E_\alpha = 40$ MeV. The reactions can be well described as a simple direct transfer of a ^3He -like cluster. The fact that the angular distributions show a J -dependence which is reproduced in the spectroscopic calculations provides a promising spectroscopic tool.

E

NUCLEAR REACTIONS $^{16}\text{O}, ^{12}\text{C}(\alpha, n), E = 41$ MeV; measured $\sigma(E_n, \theta)$; $^{19}\text{Ne}, ^{15}\text{O}$ deduced levels. TOF spectrometer.

1. Introduction

In the study of multi-nucleon transfer reactions for which the projectile energy is sufficiently high, approximately 10 MeV per nucleon, the data suggest that the nucleons are transferred as a cluster and that the states populated in the final nucleus have a large overlap with this cluster moving about an inert core. For three- and four-nucleon transfer on light nuclei, the spectra display characteristics of rotational bands. A variety of models have been used to interpret the results including: the full shell model ¹⁻³, the SU(3) model ⁴, and the cluster model ^{5,6}.

We have studied the (α, n) reaction on ^{12}C and ^{16}O to determine whether, due to the simplicity of the projectile and ejectile, more detailed spectroscopic information can be extracted using the (α, n) reaction than can be extracted from heavy-ion induced ^3He transfer reactions. It is also of interest to compare the results with those from the (α, p) reaction on the same targets ^{7,8}.

2. Experimental

The data were collected using the neutron time-of-flight spectrometer ⁹) associated with the University of Michigan 83 inch cyclotron. The floor plan is shown in fig. 1. Briefly, with this spectrometer, a measurement is made of the time for a

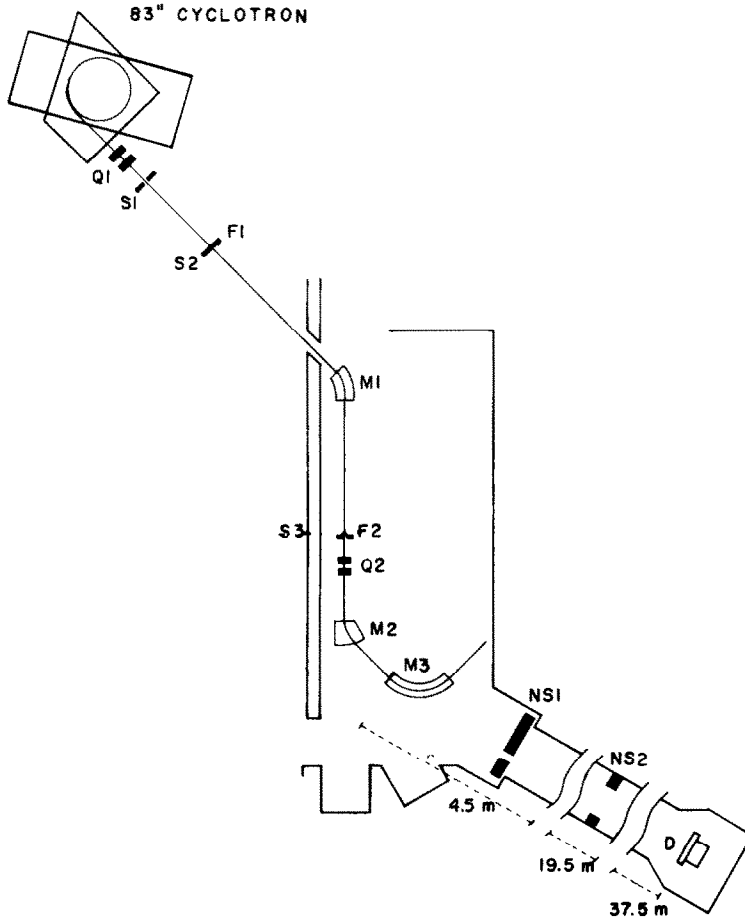


Fig. 1. Floor plan of the time-of-flight facility. See the text for identification of symbols.

neutron to travel the known distance from its point of origin in the target located in M3 to the detector D.

The cyclotron provides narrow bursts of charged particles which pass through the beam transport system (elements Q1 to M3) and strike the target located in the gap of the “target” magnet M3. The neutron scattering angle, measured with respect to the charged particle beam impinging on the target, is varied by varying the azimuthal position of the target in the magnet M3 while keeping the detector fixed.

In the usual mode of operation of an isochronous cyclotron the accelerated beam is bunched in time with repetition rate of the pulses equal to the rf frequency. For the 41 MeV α -particle beam accelerated in the 83 inch cyclotron the period of the rf is about 130 ns. Since the time-of-flight of the neutrons of interest over a 37 m flight path ranges from 500 to 1500 ns, the normal repetition rate is too high. It was

reduced by means of a gated ion source¹⁰). The time-of-flight technique also requires that the particles in each pulse come from the same turn in the accelerating cycle. The details of obtaining single turn extraction are described elsewhere¹¹).

The energy resolution ($\Delta T/T$) of the spectrometer for a flight time t is in lowest order ($\Delta T/T$) = 2($\Delta t/t$). A more accurate expression, including relativistic effects, is

$$(\Delta T)^2 = (\Delta E)^2 + \frac{(299.8)^2}{l^2} (\Delta t)^2 \left[\frac{T^2 + 2TE_0}{E_0^{4/3}} \right]^3 \\ + \frac{(100d)^2}{l^2} \left[2 + \frac{3T}{E_0} + \frac{T^2}{E_0^2} \right]^2 T^2,$$

where T is the neutron kinetic energy in MeV, and ΔT its uncertainty in keV, E_0 is the neutron rest mass energy in MeV, ΔE is the uncertainty in the charged particle energy in keV, l is the flight path in m, d is the uncertainty in flight path in cm and Δt is the uncertainty in flight time in ns. The three terms in the equation correspond to uncertainties in the measurement of energy, time, and flight path.

The uncertainty in the charged particle energy, ΔE , is due to the energy spread in the charged particle beam and to the energy straggling of the beam in the target system combined in quadrature. The energy spread in the 41 MeV α -particle beam was typically 40 keV (corresponding to the resolving power of the beam transport system of $E/\Delta E = 1050$), straggling in the gas cell about 130 keV, and in the solid carbon target about 80 keV.

Timing uncertainties arise as the result of the finite width of the beam pulses, the slow drift in the rf phase of the beam, time spread introduced in the beam transport system (much less than 1 ns) and the timing capabilities of the detector and the signal processing electronics. Characteristics of the detector array, including time resolution (0.90 ± 0.1 ns), efficiency and neutron- γ -ray discrimination are described elsewhere⁹). They result in a contribution to ΔT of 100 keV and 390 keV for 10 MeV and 25 MeV neutrons respectively for a 37 m flight path.

The uncertainty in flight path arises from two sources, the finite thickness of the detecting medium and flight path differences arising from the finite solid angle subtended by the detector. For the detector and geometry employed these contributions to ΔT were negligibly small compared with the contributions from the other two sources.

The practical limit on the resolution in these measurements is 0.5% and 1% for 5 and 25 MeV neutrons respectively for a detector efficiency of approximately 0.06 and using a 2 MeV low energy cut-off.

The background arises from three sources: cosmic rays and γ -rays from the surroundings, γ -rays and neutrons produced by the beam in the absence of a target, and γ -rays and neutrons produced at the target. Of these by far the largest contribution comes directly from the target structure as is illustrated by fig. 2 which shows the neutron spectrum produced by the empty gas cell. Neutrons scattered into

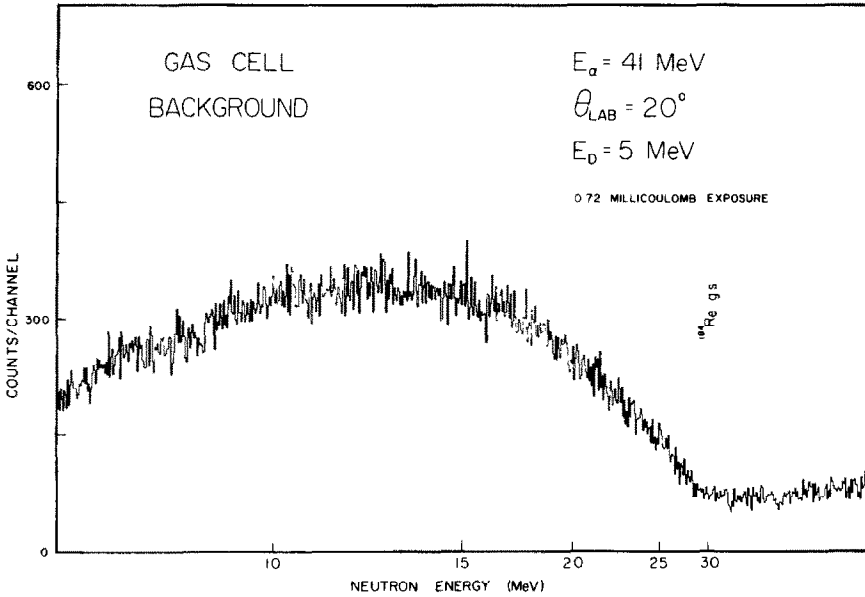


Fig. 2. Neutron background from evacuated gas cell. The rise in the background at $T_n \approx 30$ MeV corresponds with the Q -value for the $^{181}\text{Ta}(\alpha, n)^{184}\text{Re}$ reactions. The counts above 30 MeV result from low-energy neutrons from the above reaction having a flight time greater than one gating period.

the detector from the pole faces of the target magnet and the tunnel walls are minimized by two sets of slits shown in fig. 1: NS1 defines the flight path, NS2 reduces the contribution from small-angle scattering.

3. Targets

For measurements of the $^{12}\text{C}(\alpha, n)^{15}\text{O}$ reaction a self-supporting natural carbon target was constructed by stacking 12 carbon foils, each nominally $40 \mu\text{g}/\text{cm}^2$ †. The thickness as measured using an ^{241}Am α -gauge, was determined to be $480 \pm 72 \mu\text{g}/\text{cm}^2$.

For the study of the $^{16}\text{O}(\alpha, n)^{19}\text{Ne}$ reaction both a solid MoO_3 target and a gas cell were used. The MoO_3 targets were prepared by the vacuum evaporation of natural MoO_3 onto a $900 \mu\text{g}/\text{cm}^2$ Ni backing. Because the oxygen content of the target decreased with beam exposure they are used only for measurements of spectral line intensities relative to the 4.62 MeV level in ^{19}Ne . The gas cell was used to obtain the absolute angular distribution for the strong 4.62 MeV level.

The gas cell has a chamber 2.5 cm thick and windows of 0.0003" tantalum. The gas pressure was measured at room temperature using a mercury manometer, the cell

† Obtained from the Yissum Research Corp., Jerusalem, Israel.

was then sealed and installed in the vacuum chamber of the target magnet. The number density of the oxygen was determined to within $\pm 5\%$, the uncertainty being due primarily to the bowing of the gas cell windows.

4. Data reduction

The energy of the incident α -particles was measured using the high-resolution magnetic analysis system associated with the 83 inch cyclotron. The spectra were calibrated in time by recording the prompt γ -rays produced by the ungated beam striking the target so that the time interval between peaks equals the rf period. With the gated beam the pulse-shape gate was adjusted to allow a slight leakage of γ -rays to give a prompt γ -peak in the neutron spectra. The flight time for this peak is fixed by the flight path and the speed of light.

5. Experimental results

5.1. THE $^{16}\text{O}(\alpha, n)^{19}\text{Ne}$ REACTION

A neutron spectrum from the reaction $^{16}\text{O}(\alpha, n)^{12}\text{C}$ at 15° laboratory angle using the gas cell target is shown in fig. 3a. Because of the high background, due primarily to the gas cell windows, the cell was filled to a relatively high pressure, about 450 mm Hg of O_2 , resulting in a 2.2 mg/cm^2 oxygen target. As a result the energy resolution (FWHM) for the 20 MeV neutrons corresponding to the 4.62 MeV state in ^{19}Ne is about 500 keV, which makes it impossible to identify any strength above 12.5 MeV excitation energy.

A spectrum taken at 15° laboratory angle using a MoO_3 target on a thin Ni backing is shown in fig. 3b. The resolution for the 4.62 MeV state is about 360 keV and is due primarily to timing uncertainties. Absolute energy uncertainties contribute only 140 keV. The improved resolution together with the reduced background make it possible to identify some strength between 14 and 15.5 MeV excitation and between 16 and 16.5 MeV. However, the reduction of the oxygen content of the target with exposure to the beam and the rapidly changing detector efficiency with neutron energy for neutrons in this energy range make it difficult to draw further conclusions about this strength. Groups at 9.25, 10.4 and 11.1 MeV excitation were resolved. Below 9.0 MeV excitation no information in addition to that obtained with the gas cell was obtained.

The information on the neutron groups which could be clearly identified at several angles is given in table 1 together with the results from other laboratories.

Angular distributions, measured from 0° to 50° laboratory angle for the resolved groups, are shown in fig. 4. The bars on the data points represent statistical uncertainties only. The solid curves are the result of local, zero-range DWBA calculations using the code DWUCK IV [ref. ¹²].

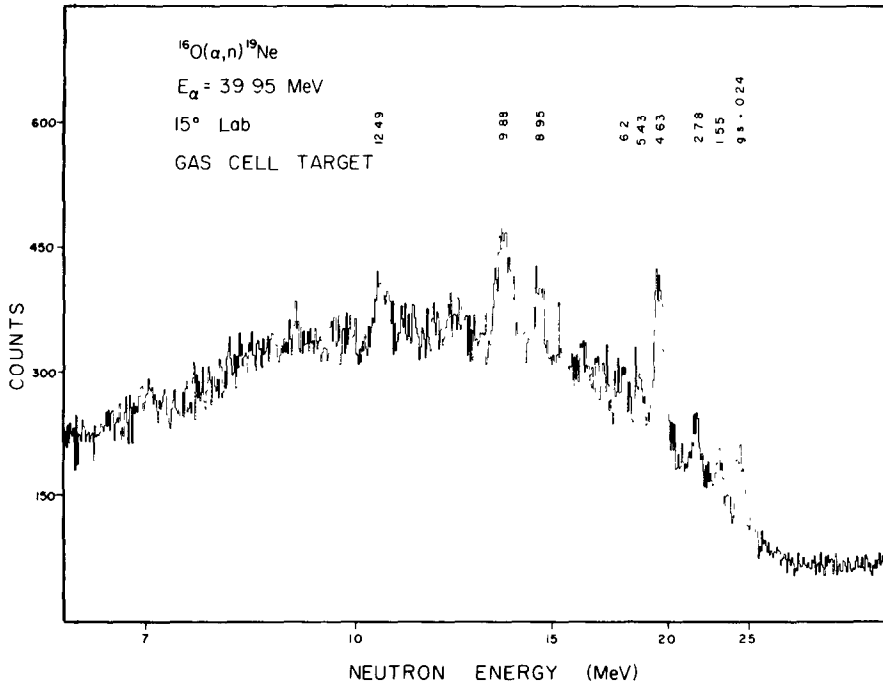


Fig. 3a. Neutron time-of-flight spectrum from the $^{16}\text{O}(\alpha, n)^{19}\text{Ne}$ reaction for the gas cell target.

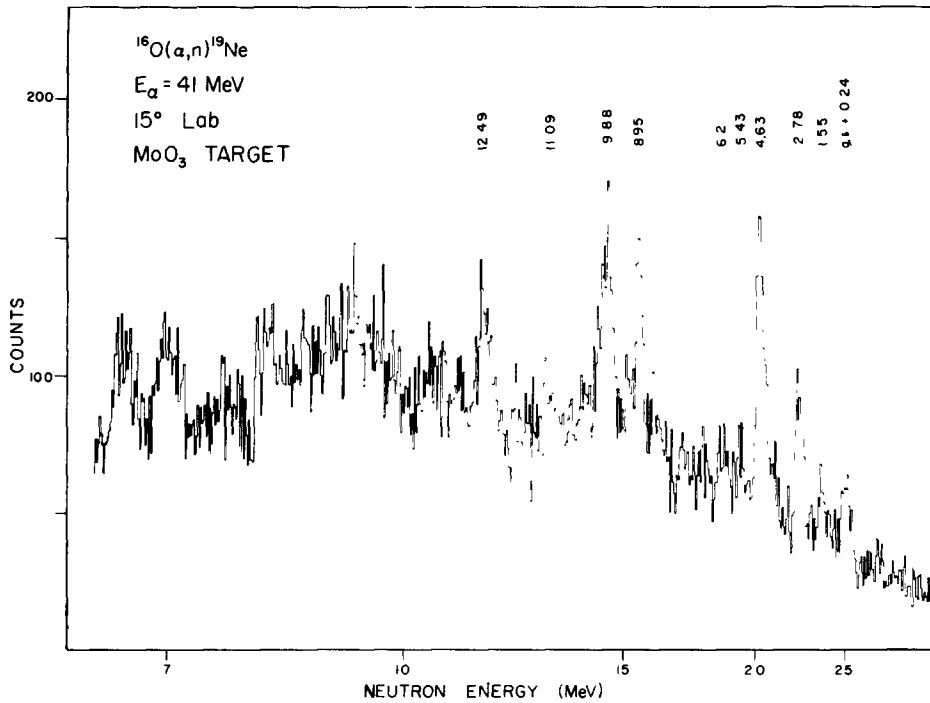


Fig. 3b. Same as fig. 3a, for MoO_3 target.

TABLE 1
 $^{16}\text{O}(\alpha, n)^{19}\text{Ne}$ results

E_x^a (MeV)	(E_x^b) (MeV)	$d\sigma/d\Omega$ (mb/sr) at 15° lab	Int. c
0.0			
0.238	0.19	0.50	26
1.55	1.55	0.32	17
2.80	2.78	0.75	34
4.21	4.20		
4.64	4.63	1.75	68
5.43	5.43	0.50	21
6.29	6.2	0.55	26
6.86	6.80	0.43	17
7.22	7.61	0.44	22
8.09			
8.45	8.42	0.34	20
8.94	8.95	0.80	31
	9.23		
9.83	9.88	1.10	55
9.99			
	10.40		
11.26	11.09		
11.38			
12.57	12.49	0.98	60

^{a)} $^{16}\text{O}(^6\text{Li}, t)^{19}\text{Ne}$ results ¹³⁾.

^{b)} This work.

^{c)} Defined as $\int_0^{60} (d\sigma/d\Omega) d\Omega$.

5.2. THE $^{12}\text{C}(\alpha, n)^{15}\text{O}$ REACTION

A neutron spectrum from the $^{12}\text{C}(\alpha, n)^{15}\text{O}$ reaction at 15° laboratory angle with $E_\alpha = 41$ MeV using a natural carbon target is shown in fig. 5. The striking feature is the fact that relatively few levels are strongly populated. A comparison of the results with a high resolution spectrum ¹³⁾ of the reaction $^{12}\text{C}(^6\text{Li}, t)^{15}\text{O}$ indicates that only the peaks at 10.48, 11.71, 12.85 and 15.05 MeV in the (α, n) spectra can be considered as transitions to a single state in ^{15}O . All other peaks contain contributions from at least two levels. In particular, the partially resolved doublet at 7.2 MeV contains a contribution from the $\frac{3}{2}^+$ state at 6.79 MeV as well as contributions from states at 6.87 and 7.28 MeV. The peak at 9.64 MeV contains contributions from at least three levels at 9.48, 9.61 and 9.66 MeV. In addition, it is probable that the peak at 5.24 MeV contains a small contribution from the $\frac{1}{2}^+$ state at 5.18 MeV.

The information on the neutron groups which could be clearly identified at several angles is presented in table 2 together with the results from other work.

Angular distributions in the range 0° to 60° laboratory angle are shown in fig. 6. The bars on the data points represent statistical uncertainties only. The solid curves are the result of a local zero-range DWBA calculation using the code DWUCK IV.

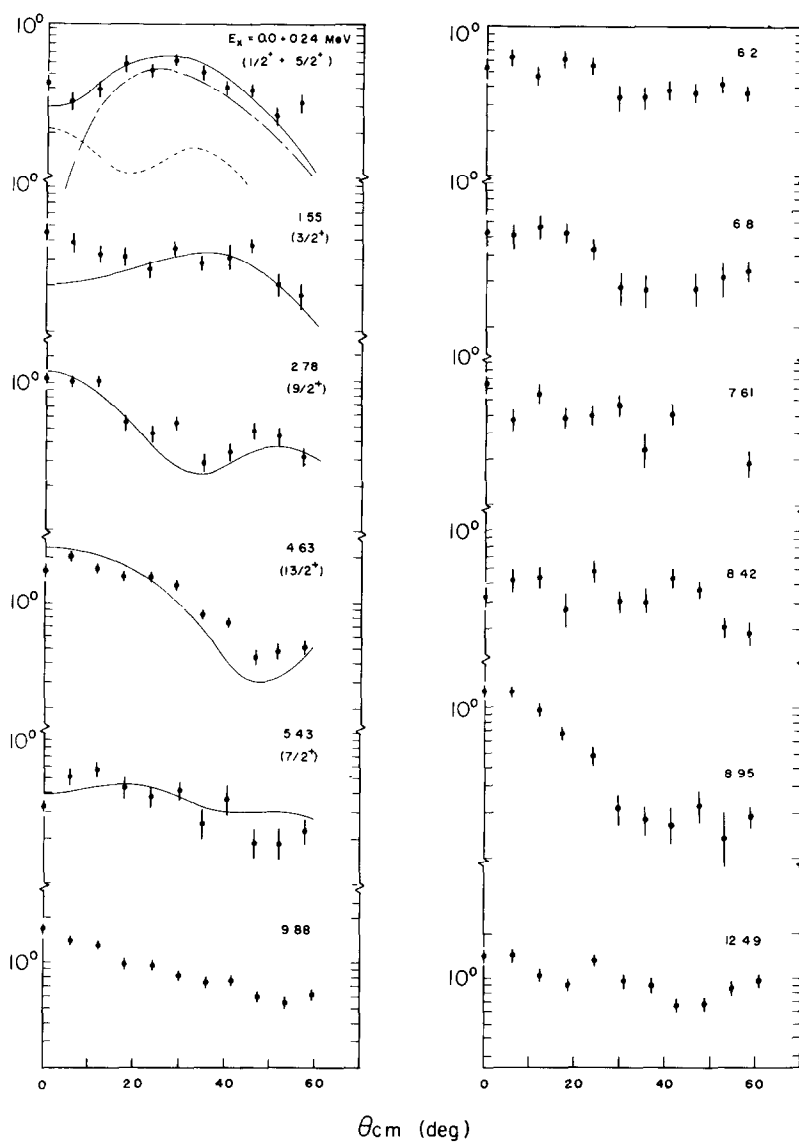
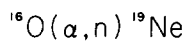


Fig. 4. Angular distributions for neutron peaks resulting from the $^{16}\text{O}(\alpha, n)^{19}\text{Ne}$ reaction. The curves are the result of zero-range DWBA calculations.

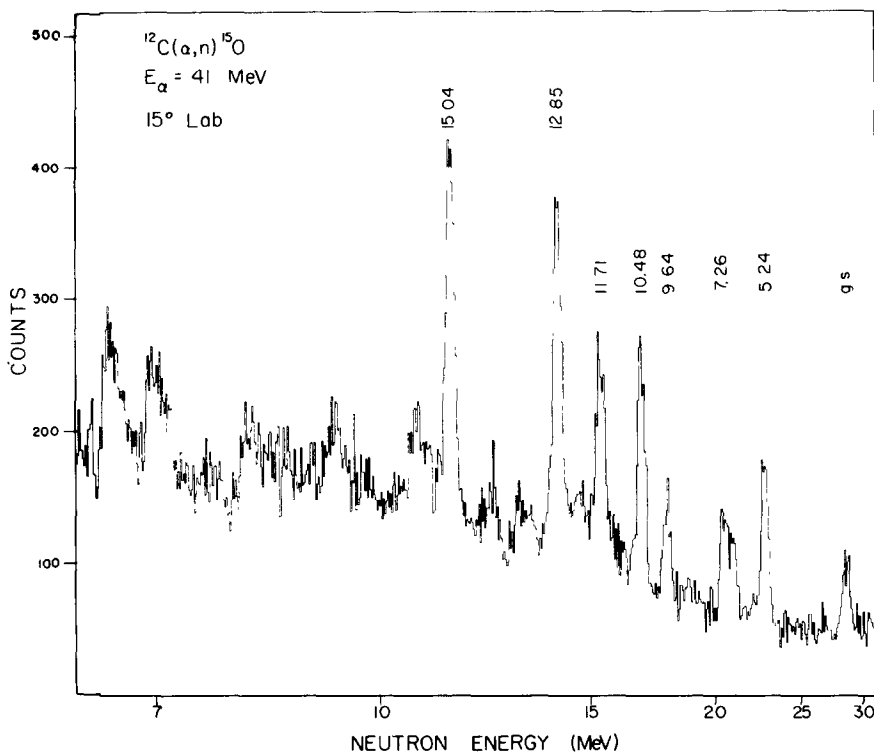


Fig. 5. Neutron time-of-flight spectrum for the $^{12}\text{C}(\alpha, n)^{15}\text{O}$ reaction.

6. Discussion

The direct nature of the (α, n) reaction is clearly shown by the following: (i) Only a few states at high excitation energy are populated in ^{15}O and ^{19}Ne . (ii) In ^{19}Ne negative-parity states at low excitation energy, for instance the $\frac{7}{2}^{-}, \frac{9}{2}^{-}$ doublet at $E_x \approx 4.2 \text{ MeV}$, are at most weakly populated in comparison with positive-parity states of the same spin. This is in agreement with expectation based on their wave functions which are dominated by $4p-1h$ components. (iii) There is no evidence for the population of the $\frac{3}{2}^{-}$ level at $E_x = 6.18 \text{ MeV}$ in ^{15}O in agreement with its wave function which is dominated by a $p_{3/2}$ hole.

6.1 DWBA ANALYSIS

The data were analyzed assuming the (α, n) reaction could be described as a direct single-step transfer of a ^3He -like cluster with zero-range interaction between the incident α -particle and the transferred ^3He which has internal quantum numbers $l=0$ and $s=\frac{1}{2}$. The DWBA calculations were carried out using the code

TABLE 2
 $^{12}\text{C}(\alpha, n)^{15}\text{O}$ results

E_x^a (MeV)	E_x^b (MeV)	$d\sigma/d\Omega$ (mb/sr) at 15° lab	Int. c
	0.0		
5.18			
5.24	5.24	0.70	32
6.18			
6.79			
6.87	6.89	0.27	
7.28	7.26	0.42	33
8.29			
8.92	8.91	0.04	
8.98			
9.49			
9.61	9.63	0.40	26
9.66			
9.76			
10.27			
10.45	10.48	0.58	34
11.15	11.1		
11.56			
11.72	11.71	0.80	35
11.98			
12.3	12.3		
12.6			
12.84	12.85	1.15	48
	13.45		
13.55			
		0.27	
13.75	13.72		
14.27	14.27	0.17	
15.05	15.05	1.20	64
15.48			
15.60	15.65	0.32	
15.65			
15.80			

^{a)} $^{12}\text{C}(^6\text{Li}, t)^{15}\text{O}$ results ¹³⁾.

^{b)} This work.

^{c)} Integrated cross section defined as $\int_0^{75} (d\sigma/d\Omega) d\Omega$.

DWUCK ¹²⁾. The relation between the experimental and theoretical cross section for these calculations is given by

$$\left(\frac{d\sigma}{d\Omega}\right)_{\text{exp}} = C \frac{2J_f + 1}{(2J_i + 1)(2J + 1)} \left(\frac{d\sigma}{d\Omega}\right)_{\text{DWBA}} \quad (1)$$

The normalization constant, C , contains all the spectroscopic information as well as several factors which, for a given reaction, are independent of the particular

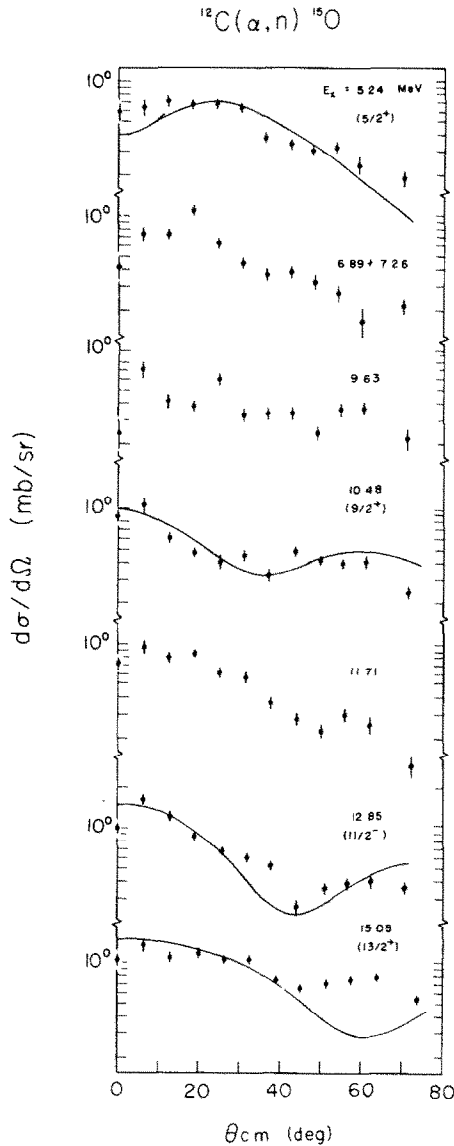


Fig. 6. Angular distributions for neutron peaks resulting from the $^{12}\text{C}(\alpha, n)^{15}\text{O}$ reaction. The curves are the results of zero-range DWBA calculations.

transition under consideration. Therefore, if a transition can be thought of as proceeding with a particular value of $Q = 2N + L$, the factor C could be proportional to the spectroscopic factor if the form factor and wave functions of the incoming and outgoing waves are adequately described.

Cluster form factors were constructed in a Woods-Saxon well assuming a ^3He cluster in an internal $(0s)$ state with quantum numbers $(n, l, j) = (0, 0, \frac{1}{2})$ and the

relative motion described by the quantum numbers N, L, J with a binding energy equal to the ^3He separation energy. For states unbound with respect to ^3He , a binding energy of -0.5 MeV was used. The shapes and magnitudes of the calculated angular distributions, especially for those with $J = L - S$, were very sensitive to the bound state parameters, especially the diffuseness parameter and the strength of the spin-orbit potential. Reasonable fits to the data could be obtained only for $a \approx 0.5$ which is considerably smaller than the usual $a \approx 0.75$ listed for ^3He optical model parameters. This may result from the inappropriateness of the use of the Woods-Saxon potential to describe rotational states as was pointed out by Buck and Pilt⁶⁾.

The optical-model parameters used to describe the entrance and exit channels in the $^{16}\text{O}(\alpha, n)^{19}\text{Ne}$ and $^{12}\text{C}(\alpha, n)^{15}\text{O}$ reactions are listed in table 3. The neutron parameters were calculated according to the Becchetti-Greenlees formula¹⁴⁾. The α -particle parameters are the same as those used to analyze the $^{16}\text{O}(\alpha, p)^{19}\text{F}$ reaction¹⁵⁾. The calculated fits are sensitive to the α -particle parameters and relatively insensitive to the neutron parameters. The reason for the success of this set of α -particle parameters may be that they satisfy quite well the well-matching conditions of DelVecchio¹⁶⁾.

TABLE 3
Optical-model parameters

	V_r	r_c	r	a	W	W_D	r_I	a_I	$V_{s.o.}$	$r_{s.o.}$	$a_{s.o.}$
α	199.1	1.25	1.262	0.65	42.17		1.262	0.65			
$n^{12}\text{C}$	48.4		1.17	0.75	4.67	6.675	1.26	0.58	6.2	1.01	0.75
$n^{16}\text{C}$	49.6		1.17	0.75	3.9	7.375	1.26	0.58	6.2	1.01	0.75
^3He		1.25	1.22	0.52					$\lambda = 5$		

The normalization constant, C , defined in eq. (1) was found for the transitions which could be fit with a calculated curve by visually adjusting the calculated curve to the data. The results are listed in tables 4 and 5 for ^{19}Ne and ^{15}O .

TABLE 4
Normalization constants extracted from $^{16}\text{O}(\alpha, n)^{19}\text{Ne}$

E_x	J^π	C	
		(α, n)	$(\alpha, p)^a)$
0.0	$\frac{1}{2}^+$	72 ^{b)}	
0.238	$\frac{3}{2}^+$	72 ^{b)}	91
1.54	$\frac{3}{2}^+$	141	59
2.79	$\frac{9}{2}^+$	87	77
4.62	$\frac{13}{2}^+$	254	244
5.4	$\frac{7}{2}^+$	142	77

^{a)} For analog states in ^{19}F [ref. 8)].

^{b)} Assuming the same C for the g.s. and 0.238 levels.

TABLE 5
Normalization constants extracted from $^{12}\text{C}(\alpha, n)^{15}\text{O}$

E_x	J^π	$2N+L$	C
5.24	$\frac{5}{2}^+$	4	155 ^{a)}
5.24	$\frac{5}{2}^+$	6	35 ^{a)}
10.45	$\frac{9}{2}^+$	6	64
12.85	$\frac{11}{2}^-$	5	270
15.05	$\frac{13}{2}^+$	6	296

^{a)} Assuming all strength is due to that particular $2N+L$ value.

The DWBA calculations predict a J -dependence in the angular distribution for $J \leq \frac{9}{2}$ and the angular distributions for the $J^\pi \leq \frac{9}{2}^+$ members of the ground-state rotational band in ^{19}Ne exhibit a J -dependence. Note for example in fig. 4 the difference in the shapes of the $L = 2$ transitions to the $\frac{3}{2}^+$ and $\frac{5}{2}^+$ members at $E_x = 1.54$ and 0.23 MeV and also of the $L = 4$ transitions to the $\frac{7}{2}^+$ and $\frac{9}{2}^+$ members at $E_x = 5.4$ and 2.79 MeV. Because angular distributions could not be extracted for a doublet in ^{15}O , J -dependence for the $^{12}\text{C}(\alpha, n)^{15}\text{O}$ reaction was not demonstrated.

6.2. THE $^{16}\text{O}(\alpha, n)^{19}\text{Ne}$ REACTION

The relative spectroscopic factors, defined as the normalization constant C relative to the $C = 87$ value for the $J^\pi = \frac{9}{2}^+$ state at $E_x = 2.79$ MeV, are listed under S_{DW} in table 6 together with calculated values for members of the ground-state rotational band. The values for $J^\pi \leq \frac{9}{2}^+$ members are in good agreement. Two factors may contribute to the relatively large values for the $\frac{3}{2}^+$ and $\frac{7}{2}^+$ states. First it is likely that these states contain unresolved contributions from other states, and second, since the magnitude of the calculated distributions was more sensitive to the form factor parameters for transitions with $J = L - S$, the large values for these states may indicate that the form factor parameters used were not optimum.

TABLE 6
Relative spectroscopic factors for some states in ^{19}Ne [ref. 17)]

J^π	E_x	KK ¹⁸⁾	KB ¹⁹⁾	Kuo ²⁰⁾	PW ²¹⁾	S_{DW}
$\frac{1}{2}^+$	0.0	1.23	1.17	1.05	1.23	0.83
$\frac{3}{2}^+$	0.238	0.93	0.95	1.03	1.0	0.83
$\frac{5}{2}^+$	1.54	0.85	0.97	0.89	1.0	1.62
$\frac{7}{2}^+$	2.79	1.00	1.00	1.00	1.0	1.0
$\frac{9}{2}^+$	4.62	0.79	0.85	0.87	0.88	2.92
$\frac{11}{2}^+$	5.4	0.92	0.85	0.09	0.98	1.63

Note: All values are relative to that of the $\frac{9}{2}^+$ state at 2.79 MeV excitation.

The large value of the normalization constant for the $\frac{13}{2}^+$ state is disturbing. The small predicted cross section results from the fact that the form factor for this transition has zero nodes resulting in a much smaller value in the surface region than, for example, that of the $\frac{9}{2}^+$ state. This could be an indication that a pure (sd)³ description of this state is inadequate and that excitation into the fp shell must be included in its wave function. It was found that a small, approximately 10%, admixture was sufficient to obtain quantitative agreement between the calculated and experimental *S*-values.

The SU(3) (60) strength is nearly exhausted in the above states with the exception of a second $J^\pi = \frac{13}{2}^+$ having 30% to 40% of the (60) $\frac{13}{2}^+$ strength and predicted to lie at $E_x = 9\text{--}10$ MeV and the (60) $\frac{11}{2}^+$ strength. An $\frac{11}{2}^+$ state with about 40% of the $\frac{11}{2}^+$ strength is also predicted to lie at 9–10 MeV. The analogs of these states in ^{19}F have been identified at $E_x = 10.42$ and 9.9 MeV [ref. ⁸]. It is likely that they are contained in the broad peak at $E_x = 9.88$ MeV.

Since this reaction populates states of maximum spatial symmetry, the remaining strength must arise from the (sd)²(fp), (sd)(fp)², and (fp)³ configurations belonging to the leading (70), (80) and (90) representations of SU(3). A cluster model calculation by Buck and Pilt ⁶) and a rotational model calculation predict the band heads of the (70) and (80) bands at about $E_x = 7$ and 9 MeV respectively with the (90) band head at higher excitation energy.

The levels at $E_x = 8.91$ and 12.47 MeV are of particular interest since their analogs in ^{19}F are seen in both triton and α -particle transfer reactions. In the α -transfer work ²²) these states have been interpreted as the $\frac{11}{2}^-$ and $\frac{15}{2}^-$ members of the weak coupling doublets resulting from coupling a $p_{1/2}$ hole to the 6^+ and 8^+ members of the ^{20}Ne ground-state rotational band. The $\frac{13}{2}^-$ and $\frac{17}{2}^-$ members are also observed in α -transfer work but not in triton transfer. In the triton transfer work these states have been assigned as the $\frac{11}{2}^-$ and $\frac{15}{2}^-$ members of the $2N + L = 7$ band based on the fits of the calculated angular distributions with a $2N + L = 7$ form factor and the predicted excitation energies of these states. If this interpretation is correct, there must be considerable mixing between $p^{-1}(\text{sd})^4$ and $(\text{sd})^2(\text{fp})$ components in the wave functions of these states. The fact that the $\frac{13}{2}^-$ and $\frac{17}{2}^-$ members of the doublets are not seen in three nucleon transfer can be qualitatively understood in terms of a three-nucleon cluster model with spin-orbit coupling for the cluster. States with $J = L + S$ are pushed down in energy and can mix with the members of the weak coupling doublets while states with $J = L - S$ are pushed up in energy and consequently cannot mix to the same extent.

6.3. THE $^{12}\text{C}(\alpha, n)^{15}\text{O}$ REACTION

The predicted mixing for the low-spin members of the $2N + L = 4$ and 6 bands is evidenced by the strong population of the $J^\pi = \frac{5}{2}^+$ level at $E_x = 5.24$ MeV and the weak population of the $J^\pi = \frac{5}{2}^+$ level at $E_x = 8.92$ MeV. Based solely on kinematical

considerations, the level at $E_x = 5.24$ MeV is populated much more strongly than expected while the level at 8.92 MeV is somewhat weaker than expected. The observed strength of these levels is well accounted for by the predicted constructive interference between $2N + L = 4$ and 6 transfer for the level at 5.24 MeV and destructive interference for the level at 8.92 MeV.

The high-spin members of the $2N + L = 5$ and 6 bands are expected to have greater overlap with the cluster representation. The normalization constants extracted for the $J^\pi = \frac{9}{2}^+$ and $\frac{13}{2}^+$ states at $E_x = 10.45$ and 15.05 MeV respectively are approximately the same as those for the respective states in ^{19}Ne indicating the $(\text{sd})^3$ cluster representation for these states is rather good. The normalization constants for the $\frac{13}{2}^+$ and $\frac{11}{2}^-$ levels at $E_x = 15.05$ and 11.85 MeV are approximately a factor of four greater than that of the $\frac{9}{2}^+$ level at $E_x = 10.45$ MeV. As in ^{19}Ne this may indicate that excitation into the fp shell needs to be included in their wave functions.

If the state at 11.7 MeV in this work and its analog at $E_x = 11.95$ MeV in the $^{12}\text{C}(\alpha, \text{p})^{15}\text{N}$ reaction at $E_\alpha = 40$ MeV are identified as the state seen at $E_x = 11.95$ MeV in the $^{13}\text{C}(\alpha, \text{d})^{15}\text{N}$ reaction²³), the $\frac{9}{2}^-$ assignment given for this state in the (α, d) work is probably in error since it is not excited strongly in the $(^6\text{Li}, \text{t})$ (ref. 13)], $(^{10}\text{B}, ^7\text{Li})$ [ref. 24)] and $(^{12}\text{C}, ^9\text{Be})$ [ref. 25)] reactions as it would be expected to be. An $L = 3$ assignment would then be consistent with the above results. On the other hand it is possible that different states are populated in the two and three nucleon transfer reactions. This would allow an $L = 4$ assignment for this transition which would also explain the difference in the relative strengths between the heavy-ion and α -particle induced transfers.

7. Conclusions

To within the experimental energy resolution, the same states are populated in the (α, n) reaction as in the heavy-ion induced reactions on the same targets. The differences in the relative intensities can be explained in terms of the reaction kinematics. A comparison of our results for the (α, n) reaction with those of the (α, p) reaction at $E_\alpha = 40$ MeV on the same targets show good agreement based on what is expected for analog reactions on self-conjugate nuclei.

Several features observed⁸) in the $^{16}\text{O}(\alpha, \text{p})^{19}\text{F}$ reaction at $E_\alpha = 40$ MeV indicate that it can provide more detailed spectroscopic information than can be extracted from a heavy-ion induced triton transfer reaction. Among the more significant of these are: (i) The reaction mechanism at $E_\alpha = 40$ MeV can be well described as the direct transfer of a triton-like cluster with internal quantum numbers $l = 0$ and $s = \frac{1}{2}$. (ii) The shape of the angular distributions for states with $J^\pi \leq \frac{9}{2}$ is characterized by the transferred J rather than the transferred L . (iii) The shapes of the angular distributions are dependent on the $2N + L$ value of the form factor dominating the transfer. (iv) A one-step DWBA calculation reproduces these effects and yields fits to

the data. We would expect these features to be evident in the (α, n) reaction also since, except for Coulomb effects, it is identical to the (α, p) reaction.

It would appear that the $^{12}\text{C}(\alpha, n)^{15}\text{O}$ and $^{16}\text{O}(\alpha, n)^{19}\text{Ne}$ reactions can be well described as the simple direct transfer of a ^3He -like cluster with internal quantum numbers $l = 0$ and $s = \frac{1}{2}$. The calculated angular distributions, using a zero-range one-step DWBA calculation, are sensitive to the choice of ^3He bound state parameters. Calculations for transitions with $J = L - S$ were found to be more sensitive than those with $J = L + S$.

The J -dependence of the shape of the angular distributions at this α -particle energy is a promising spectroscopic tool. The fact that this feature is reproduced in the calculations emphasizes this. This feature is also found in the (α, p) reaction at $E_\alpha = 40$ MeV but is absent at 100 MeV [ref.²⁶].

The good agreement between the calculated and experimental relative spectroscopic factors for $J^\pi \leq \frac{9}{2}^+$ members of the ground-state rotational band in ^{19}Ne indicates that the leading (60) representation of the SU(3) group works quite well for these states. The results for the $\frac{13}{2}^+$ level at $E_x = 4.62$ MeV indicate that a small (sd)(fp)² admixture needs to be included in its wave function.

The importance of interference effects in determining the strengths of transitions is clearly shown in the relative strengths of the $J^\pi = \frac{5}{2}^+$ levels at $E_x = 5.24$ and 8.92 MeV in ^{15}O . The large normalization constants extracted for the $J^\pi = \frac{13}{2}^+$ and $\frac{11}{2}^-$ levels at $E_x = 15.05$ and 12.85 MeV relative to that of the $\frac{9}{2}^+$ level at 10.45 MeV indicates that excitation into the fp shell may need to be included in the wave functions of these states. The strong population of the level at $E_x = 11.7$ MeV in this work compared with its weak population in heavy-ion induced studies suggests that this transition is an $L = 3$ or 4. Therefore it is likely that either two different states are populated in two and three nucleon transfer at this excitation energy or that the $\frac{9}{2}^-$ assignment of the $^{13}\text{C}(\alpha, d)^{15}\text{N}$ work is in error.

We want to express our appreciation to K.T. Hecht for the many long and fruitful discussions on the interpretation of the data. We wish also to thank W.E. Downer and J.A. Koenig for their expert technical assistance during the course of the experiment.

References

- 1) Y. Akiyama, A. Arima and T. Sebe, Nucl. Phys. **A138** (1969) 273;
J.B. McGrory and B.H. Wildenthal, Phys. Rev. **C7** (1973) 974
- 2) E.C. Halbert, J.B. McGrory and B.H. Wildenthal, Phys. Rev. Lett. **20** (1968) 1112
- 3) A.P. Zucker, B. Buck and J.B. McGrory, Phys. Rev. Lett. **21** (1968) 39
- 4) J.P. Elliott, Proc. Roy. Soc. **A245** (1955) 128; 562;
M. Harvey, in Advances in nuclear physics, ed. M. Baranger and E. Vogt (Plenum, New York, 1968) vol. 1, p. 67
- 5) B. Buck, C.B. Dover and J.P. Vary, Phys. Rev. **C11** (1975) 1803

- 6) B. Buck and A. A. Pilt, Nucl. Phys. **A280** (1977) 133
- 7) K. van der Borg, R. J. DeMeijer, A. van der Woude and H. T. Fortune, Phys. Lett. **84B** (1979) 51
- 8) K. van der Borg, R.J. DeMeijer and A. van der Borg, Nucl. Phys. **A273** (1976) 172
- 9) W.C. Parkinson, J.F. Petersen, R.H. Day, R.M. Polichar, P.F. Julien and D.C. DuPlantis, Nucl. Instr. **119** (1974) 51
- 10) R.H. Day and W.C. Parkinson, Nucl. Instr. **111** (1973) 199
- 11) W.C. Parkinson, J.F. Petersen, R.H. Day, D.C. DuPlantis, W.S. Gray and J. Barwick, Nucl. Instr. **119** (1974) 61
- 12) P.D. Kunz, University of Colorado, unpublished
- 13) H.G. Bingham, M.L. Halbert, D.C. Hensley and E. Newman, Phys. Rev. **C11** (1975) 1913
- 14) F.D. Becchetti and G.W. Greenlees, Phys. Rev. **182** (1969) 1190
- 15) N. Baron, R. F. Leonard and W.M. Steward, Phys. Rev. **C4** (1971) 1159
- 16) R.M. DelVecchio and W.W. Daehnick, Phys. Rev. **C6** (1972) 2095
- 17) D.J. Millener, unpublished
- 18) A. Kallio and K. Kolltveit, Nucl. Phys. **53** (1964) 87
- 19) T.T.S. Kuo and G.E. Brown, Nucl. Phys. **85** (1965) 40
- 20) E.C. Halbert, J.B. McGrory, B.H. Wildenthal and P. Pandya, Adv. in Nucl. Phys. **4** (1971) 315
- 21) B.M. Freedom and B.H. Wildenthal, Phys. Rev. **C6** (1972) 1633
- 22) A.A. Pilt, D.J. Millner, H. Bradlow, O. Dietzsch, P.S. Fisher, W.J. Naude, W.D.M. Rae and D. Sinclair, Nucl. Phys. **A273** (1976) 189
- 23) C.C.Lu, M.S. Zisman and B.G. Harvey, Phys. Rev. **186** (1969) 1806
- 24) K. Nagatani, D.Y. Youngblood, R. Kenefick and J. Bronson, Phys. Rev. Lett. **31** (1973) 250
- 25) N. Anyas-Weiss *et al.*, Phys. Reports **12** (1974) 201
- 26) W.R. Falk, Phys. Rev. **C8** (1973) 1757